

# Circular motion subject to external alignment under active driving — nonlinear dynamics and the circle map

Andreas M. Menzel<sup>1,\*</sup>

<sup>1</sup>*Institut für Physik, Otto-von-Guericke-Universität Magdeburg, Universitätsplatz 2, 39106 Magdeburg, Germany*  
(Dated: December 13, 2022)

Hardly any real self-propelling or actively driven object is perfect. Thus, undisturbed motion will generally not follow straight lines but rather circular trajectories. We here address self-propelled or actively driven objects that move in discrete steps and additionally tempt to migrate towards a certain direction by discrete angular adjustment. Overreaction in the angular alignment is possible. This competition implies pronounced nonlinear dynamics including period doubling and chaotic behavior in a broad parameter regime. Such behavior directly affects the appearance of the trajectories, also during collective motion under spatial self-concentration.

## I. INTRODUCTION

Most theoretical studies on self-propelled or actively driven objects consider idealized entities that migrate along straight lines when undisturbed [1–10]. However, this idealization generally does not meet reality. During two-dimensional motion, for instance, on a substrate or near a surface, persistent imperfections of otherwise undisturbed objects can lead to circular trajectories. To study and emphasize the resulting effects, artificial so-called circle swimmers that show extreme deviations from axially symmetric shapes [11–13] or nonsymmetric vibrated hoppers [14, 15] were generated and investigated. Similarly, several biological objects show circle swimming, for example, alga cells that feature a defect in one of their usually two driving arms [16, 17]. If motion is achieved by rotational effects, such as the rotation of flagella in *Escherichia coli* bacteria, hydrodynamic coupling to nearby substrates and surfaces can lead to circular trajectories [18–23]. Besides, spontaneous symmetry breaking can induce persistently bent trajectories [24, 25]. While the spontaneous emergence of curved paths of propagation is an important topic [26], we here concentrate on objects featuring an inherent, permanent tendency of circular motion. Thus spontaneously emerging chiral motion is only covered by our consideration as long as it is sufficiently persistent over the time of observation.

The dynamics of such active objects propagating along circular trajectories have been analyzed theoretically in quite some detail [27–37]. It is common to implement in a minimal approach the tendency of circular motion using a constant torque or angular frequency that affects angular orientation. In the mentioned theoretical studies [27–37], the dynamics was considered as continuous in

time.

Yet and thus, another aspect is that many active objects move by successive discrete steps or other events of propulsion. Obviously, this applies to humans and animals performing discrete steps or jumps, but to some degree also to birds and fish that flap with their wings and fins [38–41]. On smaller scales, actively driven hoppers on vibrating plates move by discrete bounces [42–44]. To some extent, the run-and-tumble motion of microscopic self-driven swimming objects like the bacterium *Escherichia coli* [45] can be interpreted as discrete step-wise motion between individual tumbling events, as can the stop-shock-run dynamics of the marine alga *Pyramimonas octopus* [46]. The famous theoretical Vicsek model was formulated for discrete steps of motion [1, 47]. Variants of this model are still under intense investigation, concerning, for instance, the recent discovery of additional dynamic phases [48] or collective behavior in the presence of obstacles [49]. It has been demonstrated that finite step size can lead to unexpected types of behavior such as unidirectional laning and migrating cluster crystals [50]. These phenomena result from the overreaction that becomes possible from performing discrete and finite steps.

As a third ingredient, self-propelled objects frequently do not just migrate without any goal. Often, they tend to head towards a certain direction, for instance, when microorganisms turn towards or away from light [51] or humans follow escape routes [52].

Here, we combine the above ingredients. That is, we analyze the dynamics of individual self-propelled or actively driven objects that move in discrete steps, would generally follow circle-like trajectories, if undisturbed, but simultaneously tend to migrate towards a certain direction, for instance, to reach a (remote) target. We are interested in the various modes of behavior that result from such a combination. It turns out that this specific combination of the mentioned aspects of behavior as addressed in the following, already for simple individ-

\* a.menzel@ovgu.de

ual objects, leads to complex dynamics. Specifically, intermediate period doubling and chaotic motion emerges, depending on the strength of alignment.

## II. EQUATIONS OF MOTION

We consider the two-dimensional motion of a self-propelled or actively driven object, for instance, when moving on a substrate. The present direction of motion is parameterized by an angle  $\varphi$  that we measure from the  $x$ -axis of our Cartesian coordinate frame.  $\varphi$  is updated from each time step  $n$  to the next one according to

$$\varphi_{n+1} = \varphi_n + \omega + A \sin \varphi_n. \quad (1)$$

Once  $\varphi$  leaves the interval  $[0, 2\pi[$ , we map it back by adding  $\pm 2\pi$ . In this description,  $\omega$  determines the angular frequency by which  $\varphi$  changes in a discrete way, scaled by the duration of the time step. This is consistent with setting a constant torque in previous continuous models of circular self-propulsion [27–29, 31–37]. To illustrate our results in the following, we mostly select one specific value of  $\omega = \pi/5$ , leading to closed kinked trajectories of the shape of a regular polygon, see Fig. 1(a), in analogy to the smooth circles appearing in the continuous case. In fact, polygon-shaped trajectories have recently been triggered for certain light-sensitive microswimmers [53]. Testing other commensurate values of  $\omega$ , we generally recovered the qualitative signature of our results. When incommensurate values of  $\omega$  are considered, particularly irrational multiples of  $\pi$ , the regular polygon in Fig. 1(a) appears smeared to a circle of finite thickness when the trajectory over many cycles overlays itself. We illustrate an example of  $\omega = \pi/\sqrt{26}$  by the brighter curve in the background of Fig. 1(a). In the following cases, the curves for the two values of  $\omega$  appear qualitatively similar, apart from quantitative deviations due to the slightly shifted magnitude of  $\omega$  from  $\pi/5$  to  $\pi/\sqrt{26}$ . Depending on the magnitude of the tendency of alignment  $A$ , these quantitative deviations can, however, become quite significant, as illustrated below.

Most importantly, the parameter  $A$  heading the last term in Eq. (1) is associated with the strength of external alignment tendency. For straight-moving objects, that is, for  $\omega = 0$ ,  $A > 0$  in the continuous case will generally induce a heading towards the negative  $x$ -direction  $-\hat{\mathbf{x}}$  given by  $\varphi = \pi$ . Such an alignment could be induced, for example, magnetically for magnetic self-propelled Janus particles [54–56] or magnetotactic bacteria [57–59]. Another situation corresponds to a remote target far away in the direction  $-\hat{\mathbf{x}}$  that the self-propelled or actively driven object tries to reach. This could be a source of nutrient or the only exit under confinement. In our discretized consideration, this tendency of alignment along the direction  $-\hat{\mathbf{x}}$  becomes apparent for  $\omega = 0$  at small values of  $A$ , see Fig. 1(b). For larger magnitudes of  $A$ , overreactions in alignment towards  $-\hat{\mathbf{x}}$  can occur in our

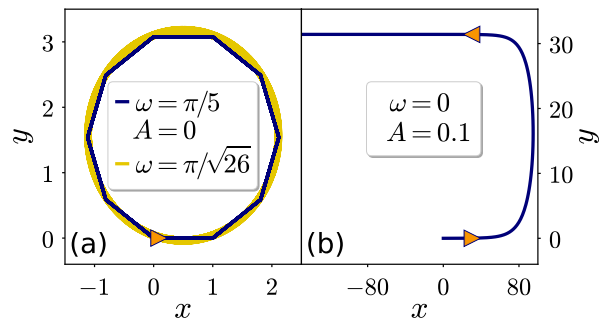


FIG. 1. Trajectories for two extreme cases. (a) Vanishing tendency of alignment  $A = 0$  for angular frequency  $\omega = \pi/5$  (darker polygon-shaped line). We observe a closed regular trajectory of discrete steps. Superimposing many cycles for  $\omega = \pi/\sqrt{26}$ , a circular shape of finite thickness emerges (brighter, thicker line in the background). (b) Vanishing angular frequency  $\omega = 0$  for alignment tendency  $A = 0.1$ . In our case, the driven object tends to orient its migration direction along  $-\hat{\mathbf{x}}$ , corresponding to  $\varphi = \pi$ . Triangles indicate the direction of motion.

discretized description. Qualitative effects on the dynamics of self-propelled particles caused by such overreactions can be substantial, as outlined before in a different context [50]. We remark that, in the continuous case, variants of Eq. (1) have been studied, for instance, in the context of flagellar synchronization [60] and of the transition to upstream swimming of sperm cells [61] and bacteria [62] near surfaces.

The actual motion of our object follows from a propulsive step

$$x_{n+1} = x_n + \cos \varphi_n, \quad (2)$$

$$y_{n+1} = y_n + \sin \varphi_n. \quad (3)$$

In these relations, we have scaled the spatial positioning by the duration of the time step and the migration speed. Both are assumed to be constant [1].

We solve Eqs. (1)–(3) by direct numerical iteration. As an initial condition, we start from a heading towards  $+\hat{\mathbf{x}}$  ( $\varphi_0 = 0$ ), unless mentioned otherwise. We note that Eq. (1) basically represents an overdamped type of dynamics for the angular variable, which sets the velocity orientation. Thus, this approach cannot reproduce phenomena that originate when inertial effects associated with angular momentum become important, as described, for instance, in the context of the turning dynamics of flocks of birds [63, 64] or so-called “microflyers” [36, 65].

## III. DIFFERENT TYPES OF TRAJECTORIES

When evaluating Eqs. (1)–(3), we made an unanticipated observation. We expected on the basis of Figs. 1(a) and (b) a combination of cyclic motion with superimposed drift, that is, a discrete version of a cycloidal-like trajectory. In fact, such types of trajectories are found

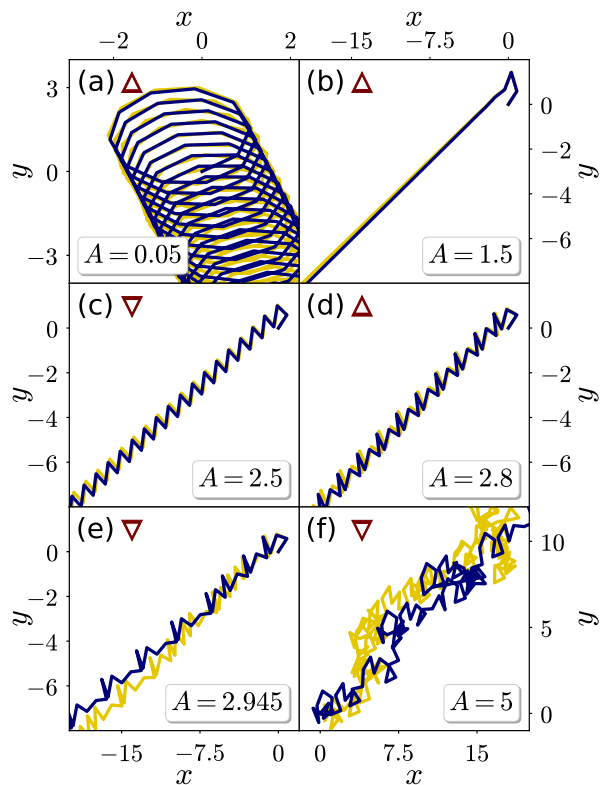


FIG. 2. Trajectories according to Eqs. (1)–(3) for combinations of nonvanishing angular frequency  $\omega = \pi/5$  and tendency of alignment  $A \neq 0$  (darker lines). (a) Cycloidal-like trajectories are observed for small but nonvanishing  $A$ , here  $A = 0.05$ . (b) For  $A = 1.5$  we find straight motion with a constant angle of deviation from  $-\hat{x}$ . (c) From there, for increasing  $A$ , regular zigzag-like trajectories appear, as depicted for  $A = 2.5$ . We observe non-binary zigs and zags with further increasing  $A$ , here for (d)  $A = 2.8$  and (e)  $A = 2.945$ . (f) Chaotic motion emerges, for example, for  $A = 5$ . The triangular arrows next to each panel label indicate whether the top or bottom abscissa scale applies. Brighter lines in the background show, for comparison, results for  $\omega = \pi/\sqrt{26}$ .

for various parameter combinations, see Fig. 2(a). Yet, further types of trajectory result, such as straight lines, although oblique to the direction of preferred alignment, see Fig. 2(b). Moreover, regular zigzag-like trajectories appear, see Fig. 2(c), besides trajectories of more complex zigs and zags, see Figs. 2(d) and (e). In many parameter regimes, we found very irregular types of trajectory, see Fig. 2(f), although we are working with a very simple deterministic system.

How can we understand these observations? In fact, it turns out that Eq. (1) corresponds to a famous minimal model studied in the context of nonlinear dynamics. It is the so-called Arnol'd circle map [66]. Aspects of its properties, for example the resulting bifurcations and transitions to chaotic behavior, have been analyzed in detail [67–71]. Here, the equation, instead of being formulated as a purely mathematical model, arises naturally from a physical context when combining circular motion and the

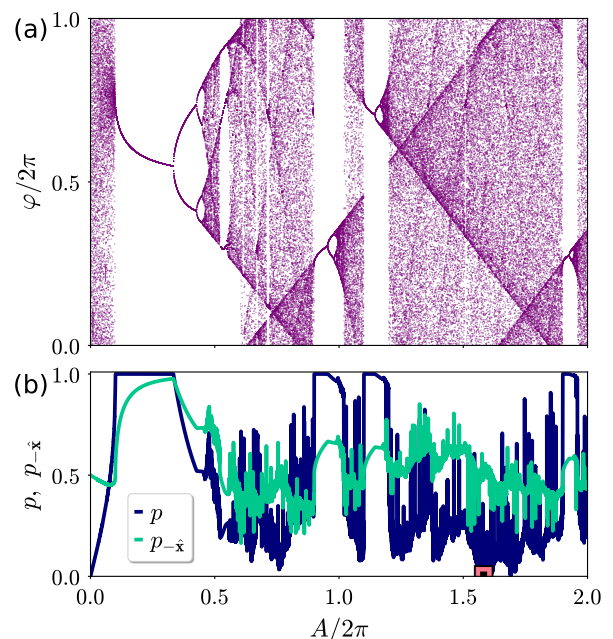


FIG. 3. Overview of the circle map. (a) Numerical evaluation of Eq. (1) for  $\omega = \pi/5$  in the interval  $0 \leq A \leq 4\pi$ . While periodic behavior exists at  $A = 0$  and in several additional intervals of  $A$ , we observe period doubling and pronounced intervals of chaotic motion as well. This map was obtained by plotting the result of  $10^4$  iterations of Eq. (1) for each value of  $A$ , after previous  $10^4$  steps of iteration. (b) Order parameters  $p$  and  $p_{-\hat{x}}$  according to Eqs. (4) and (5) for  $N_{\text{step}} = 10^4$ . We mark by the cut square the relatively low value of the order parameter  $p \approx 0.0066$  at  $A = 9.940441$  used in Figs. 5 and 6.

tendency of moving towards a preferred direction. While the circle map does feature periodic intervals, phenomena of period doubling and chaotic behavior emerge as well. We include an evaluation of Eq. (1) for the interval  $0 \leq A \leq 4\pi$  in Fig. 3(a) for illustration. In our context, these results get transformed into trajectories in the two-dimensional plane as described in the following.

At precisely  $A = 0$ , periodic behavior is found, which leads to the regular polygon-like trajectory in Fig. 1(a) for  $\omega = \pi/5$ . For slightly larger values  $A \gtrsim 0$ , the distance between the cyclic values of  $\varphi$  starts to deviate from exactly  $\omega = \pi/5$ . Consequently, the spectrum of  $\varphi$ -values in Fig. 3(a) gets broadened, corresponding to cycloidal-like trajectories as in Fig. 2(a).

The map in Fig. 3(a) illustratively explains the remaining behavior observed in Fig. 2. Intermediate  $A$ -intervals are characterized by a single recurrent value of the angle  $\varphi$ . These intervals indicate a fixed angular orientation, yet generally oblique to the preferred direction  $-\hat{x}$ , see Fig. 2(b). Apparently, the tendencies of rotation set by  $\omega$  and of alignment set by  $A$  here balance each other, compromising to an offset angle  $\varphi \neq \pi$ . Such intervals are with increasing  $A$  followed in Fig. 3(a) by events of period doubling. After the first doubling, two alternating angles are associated with zigzag-type motion, see

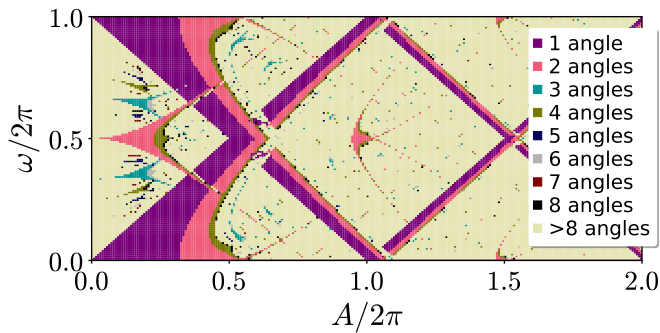


FIG. 4. Overview on the different dynamic regimes in the steady state observed when varying the angular frequency  $\omega$  and the tendency of alignment  $A$ . We distinguish between types of behavior for which repeated evaluations of Eq. (1) lead to one [see Fig. 2(b)], two [see Fig. 2(c)], three, four [see Fig. 2(d)], five, six, seven, eight [see Fig. 2(e)], or more different values of  $\varphi$ . The latter case is predominantly associated with chaotic behavior [see Fig. 2(f)] in our resolution. We set the tolerance when testing whether angles are identical to  $\pm\pi/1000$ .

Fig. 2(c). More complex trajectories result after further period doubling, which translates into different zigs and zags, see Figs. 2(d) and (e). Finally, the broad intervals of obviously chaotic behavior in Fig. 3(a) are reflected by the rather irregular appearance of associated trajectories, see Fig. 2(f).

Mainly, we focus on the values of the angular frequency  $\omega$  as indicated above and in the captions of Figs. 1–3. Yet, to briefly demonstrate how the different dynamic regimes as illustrated in Figs. 2 and 3 are affected when varying  $\omega$ , we include Fig. 4. There, we test for the dynamic behavior for which Eq. (1) in the steady state evaluates to one, two, three, four, five, six, seven, eight, or more different values of  $\varphi$  upon iteration. To our resolution, the latter case may predominantly be ascribed to chaotic behavior.

#### IV. CHARACTERIZING THE TRAJECTORIES AND TYPES OF MOTION

As a first step of quantifying the observed types of motion, we define an order parameter

$$p = \frac{1}{N_{\text{step}}} \left[ \left( \sum_{n=1}^{N_{\text{step}}} \cos \varphi_n \right)^2 + \left( \sum_{n=1}^{N_{\text{step}}} \sin \varphi_n \right)^2 \right]^{1/2}, \quad (4)$$

where the sums run over  $N_{\text{step}}$  subsequent time steps. This parameter vanishes,  $p = 0$ , in the absence of any persistent net drift towards a preferred direction. Conversely,  $p = 1$  signals persistent and fully directed motion towards a certain direction. Therefore, the drift parameter  $p$  measures how effectively the object moves forward.

In Fig. 3(b),  $p$  is plotted as the darker line. It starts

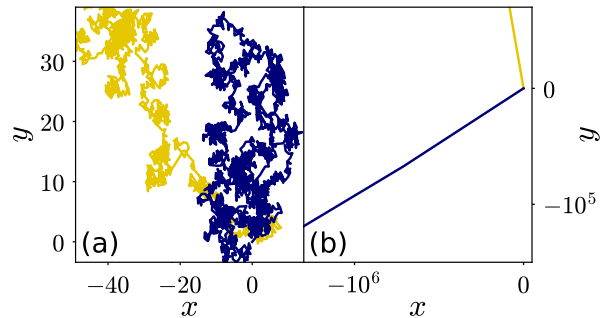


FIG. 5. Trajectory of chaotic motion for a tendency of alignment  $A = 9.940441$  for an angular frequency  $\omega = \pi/5$  (darker lines). The order parameter in Eq. (4) assumes a very low value of  $p \approx 0.0066$ , see also the square in Fig. 3(b). (a) An irregular shape appears on shorter time and length scales. (b) Conversely, the net motion towards one direction is visible on large time and length scales, where the trajectory appears rather straight. For comparison, evaluations for  $\omega = \pi/\sqrt{26}$  are included as well (brighter lines). Although the curves appear qualitatively similar in shape, the small change in  $\omega$  leads for the chosen magnitude of  $A$  to significant quantitative deviations, particularly concerning the overall drift angle in (b).

from  $p = 0$  at  $A = 0$ , in agreement with the closed trajectory that does not imply any average displacement. With increasing tendency of alignment, the object starts to drift towards a certain direction and  $p$  increases with increasing  $A$ . The motion is most effective and fully directed along one axis in intervals of only one angle in Fig. 3(a), where  $p = 1$ . Period doubling reduces  $p$ , while chaotic motion can push it to very low values. Still, we always found  $p > 0$  in these intervals, implying that a net drift motion is associated with the irregularly shaped trajectories.

To demonstrate this aspect, we concentrate on  $A = 9.940441$ , for which  $p \approx 0.0066$  is very low. Here, significant amounts of overreaction occur in individual steps of angular alignment already for weak deviations from the heading towards  $-\hat{x}$ . We plot the corresponding trajectory in Fig. 5(a) on a shorter time scale. Previous studies focusing on variants of Eq. (1) have reported diffusive behavior of the angular variable  $\varphi$  for  $\omega = 0$  [72, 73]. Considering here in addition the spatial variables, a net drift becomes obvious when we increase the time interval. Zooming out, the trajectory more and more resembles again a straight line, see Fig. 5(b). Averaging as a test over 1000 different initializations of  $\varphi_0$  in the interval of  $[0, 2\pi[$ , we still obtain  $\langle p \rangle \approx 0.0086$ , which agrees with the order of magnitude mentioned above.

Eventually, the order parameter  $p$  does not quantify whether the motion is headed towards the requested direction  $-\hat{x}$ . For this reason, we introduce a second order parameter

$$p_{-\hat{x}} = \frac{1}{2N_{\text{step}}} \sum_{n=1}^{N_{\text{step}}} (1 - \cos \varphi_n). \quad (5)$$

We obtain  $p_{-\hat{\mathbf{x}}} = 1$  when the motion is fully directed towards  $-\hat{\mathbf{x}}$  during each time step, while  $p_{-\hat{\mathbf{x}}}$  vanishes for straight motion into the opposite direction  $+\hat{\mathbf{x}}$ . In between,  $p_{-\hat{\mathbf{x}}} = 0.5$  signals that there is no net motion along  $\hat{\mathbf{x}}$ .  $p_{-\hat{\mathbf{x}}}$  is indicated in Fig. 3(b) by the brighter line. Apparently, completely directed motion along a straight line does not necessarily imply an effective motion towards the target direction  $-\hat{\mathbf{x}}$ . In our situation, we address actively driven objects of given persistent bends in their trajectories and given strengths of alignment tendency as quantified by a set magnitude of  $\omega$  and  $A$ , respectively. We thus conclude that, to achieve for such prescribed values a most effective requested propagation towards a target, it may be reasonable to work with an angular offset for the heading direction.

## V. COLLECTIVE DYNAMICS

Finally, we investigate how mutual interactions support collective and rectified motion, particularly in the chaotic regime. To this end, we consider orientational interactions of the Vicsek type [1] between  $N$  self-propelled or actively driven objects, labeled by  $i = 1, \dots, N$ . At each time step, the angle  $\varphi_i$  of the  $i$ th object is set equal to the averaged heading of all objects within a distance  $d$  from it. Obvious example systems concerning discrete collective alignment interactions are robotic swarms or otherwise artificial, programmed realizations of actively driven objects that suffer from finite refresh rates of their sensors [74]. If monitored or steered through a common, central unit [75, 76], the update may become rather simultaneous, or at least be based on simultaneously gathered information.

To obtain our results, we begin by considering only the deterministic contributions described so far. We evaluate the mentioned Vicsek-type alignment interactions before Eq. (1). Yet, we have checked that our results are qualitatively identical when switching this order. As an initialization, we iterate  $\varphi_i$  for the  $i$ th object  $iN$  times according to Eq. (1). Only then mutual angular interactions and transport are introduced. The  $N$  objects are initially distributed at random. They are confined to a square-like box of side length  $L$  under periodic boundary conditions. We here set  $\omega = \pi/5$ ,  $A = 9.940441$ ,  $d = 1$  identical for all objects, and  $L = 10$ . Increasing the number of objects  $N$  up to 1000, we have not identified qualitative variations in the collective behavior.

For quantification, we denote by  $\varphi_{i,n}$  the angular orientation of the  $i$ th object at the  $n$ th time step and evaluate the order parameters

$$P_{\text{step}} = \frac{1}{NN_{\text{step}}} \sum_{n=1}^{N_{\text{step}}} \left[ \left( \sum_{i=1}^N \cos \varphi_{i,n} \right)^2 + \left( \sum_{i=1}^N \sin \varphi_{i,n} \right)^2 \right]^{1/2}, \quad (6)$$

$$P = \frac{1}{NN_{\text{step}}} \left[ \left( \sum_{n=1}^{N_{\text{step}}} \sum_{i=1}^N \cos \varphi_{i,n} \right)^2 + \left( \sum_{n=1}^{N_{\text{step}}} \sum_{i=1}^N \sin \varphi_{i,n} \right)^2 \right]^{1/2}, \quad (7)$$

and

$$P_{-\hat{\mathbf{x}}} = \frac{1}{2NN_{\text{step}}} \sum_{n=1}^{N_{\text{step}}} \sum_{i=1}^N (1 - \cos \varphi_{i,n}). \quad (8)$$

$P_{\text{step}}$  basically measures whether (solely) at each time step all objects move into the same direction, no matter whether this direction changes over the considered overall period. Conversely,  $P$  determines the degree of directed collective motion not distinguishing between different objects and time steps. It decreases when over time the direction of ordered collective motion changes.  $P_{-\hat{\mathbf{x}}}$  again quantifies the effectiveness of motion along the preferred direction  $-\hat{\mathbf{x}}$ .

We generally observe that the initial diversification in angular distribution does not survive the averaging procedure when stochastic contributions are absent. In fact, the order parameter  $P_{\text{step}}$  approaches values close to one after an initial period of ordering in all considered cases, see Fig. 6(a). That is, at each time step (separately), all objects move basically into the same direction. However, here for  $A = 9.940441$ , this direction becomes uncorrelated in time, and  $P$  drops towards zero. It appears as if the whole crowd synchronizes and moves chaotically as one entity. Moreover, the overall motion is hardly directed into the direction  $-\hat{\mathbf{x}}$ , as signaled by  $P_{-\hat{\mathbf{x}}} \approx 0.5$ , see Fig. 6(a).

Interestingly, orientational ordering for  $A = 9.940441$  is associated with spatial concentration of the objects. We found this process of concentration independently of the number of objects  $N$ , and in all cases we started from a random spatial distribution throughout the periodic box. Thus, the spatial and orientational dynamics are significantly coupled. An example of initial distribution and subsequent spatial concentration in one spot is depicted in Fig. 6(b). This spot basically moves as one entity during further iteration, as illustrated in a video in the Supplemental Material [77]. To quantify this localization into one spot, we introduce another order parameter,

$$P_{\text{loc}} = \frac{1}{N^2 N_{\text{step}} L} \sum_{n=1}^{N_{\text{step}}} \sum_{i=1}^N \sum_{j=1}^N \left[ (x_{i,n} - x_{j,n})^2 + (y_{i,n} - y_{j,n})^2 \right]^{1/2}. \quad (9)$$

For perfect concentration of all objects into one dot, we would find  $P_{\text{loc}} = 0$ . Otherwise,  $P_{\text{loc}}$  is the larger in magnitude the more spatially distributed the particles are. During evaluation, we take into account the periodic boundary conditions and always use the minimal distance

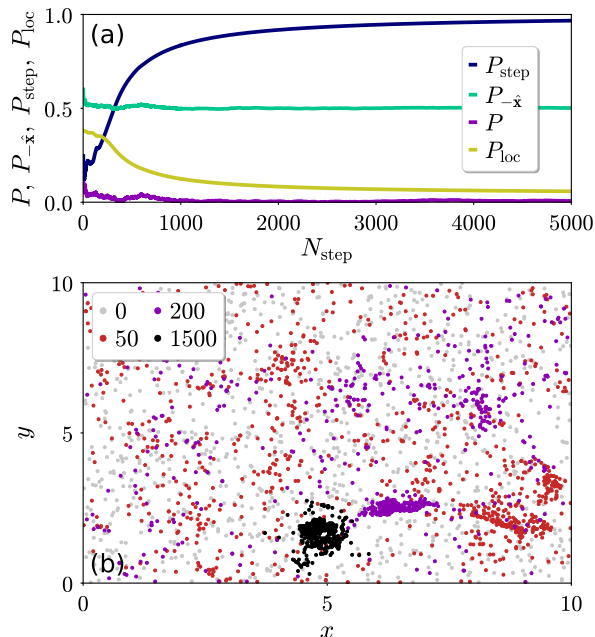


FIG. 6. Emergence of ordered collective motion in a crowd of  $N = 1000$  initially randomly arranged objects in the chaotic regime for  $\omega = \pi/5$  and  $A = 9.940441$ , see also Fig. 5. Vicsek-type mutual interactions of range  $d = 1$  in a periodic box of length  $L = 10$  are included. (a) Time evolution of the order parameters  $P_{\text{step}}$ ,  $P$ , and  $P_{-\hat{x}}$ , see Eqs. (6)–(8), indicates development of orientationally ordered collective motion ( $P_{\text{step}}$ ). Yet, the overall direction of collective motion is not correlated over time ( $P$ ) and not effectively oriented into the desired direction ( $P_{-\hat{x}}$ ). Here,  $N_{\text{step}}$  always corresponds to the total number of simulated time steps. The development of spatial concentration of the objects is quantified by the order parameter  $P_{\text{loc}}$ , see Eq. (9). (b) Positions of the objects after the amount of time steps indicated in the legend. A concentration from initial random distribution into a spot of approximate size  $d = 1$  is obvious. This spot basically moves as one entity during the further course of the dynamics [77].

between any two objects, which, depending on the situation, may be measured across the periodic boundaries.

So far, we have regarded the Vicsek-type alignment interactions as completely deterministic. In reality and generally, fluctuations and errors occur. Similarly to the Vicsek model [1], we therefore include a stochastic contribution  $\Gamma_{i,n}$  that is added to the angle  $\varphi_{i,n}$  after evaluating the alignment interactions but before evaluating Eq. (1). It accounts, for example, for the imperfections arising during the alignment procedure. We assume  $\Gamma_{i,n}$  to be uncorrelated in time, white, Gaussian distributed, and uncorrelated between the objects, so that  $\langle \Gamma_{i,n} \rangle = 0$  and  $\langle \Gamma_{i,n} \Gamma_{j,m} \rangle = 2K\delta_{ij}\delta_{nm}$ . Here,  $\delta$  denotes the Kronecker delta and  $K$  sets the strength of the stochastic contribution.

We numerically measured the time evolution of the order parameters choosing, for illustration, for  $\omega = \pi/5$  the same values of  $A$  as in Figs. 1(a), 2, and 5. Corresponding results for the magnitude of the order parameter  $P_{\text{step}}$ ,

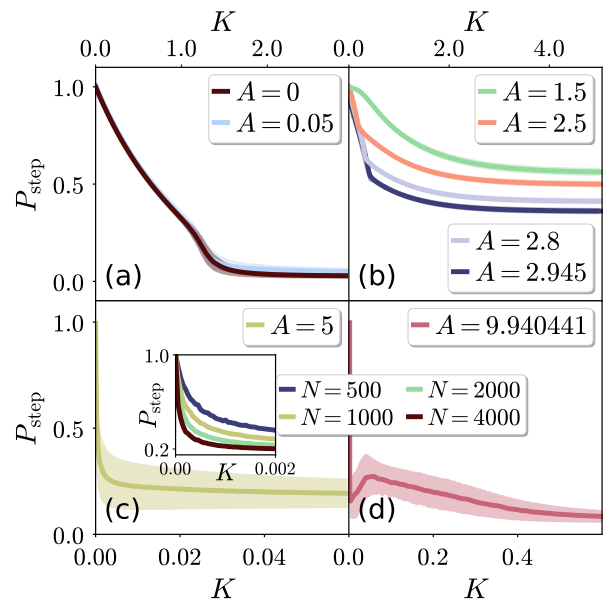


FIG. 7. Influence of additional stochastic contributions of strength  $K$  to the angular alignment of each object, superimposed before evaluating Eq. (1), on the magnitude of the resulting order parameter  $P_{\text{step}}$  in a crowd of  $N = 1000$  objects and  $\omega = \pi/5$ . For illustration, the values of  $A$  are set to (a) 0 and 0.05, (b) 1.5, 2.5, 2.8, and 2.945, (c) 5, and (d) 9.940441, as in Figs. 1(a), 2, and 5. Apparently, the sensitivity with respect to stochastic contributions significantly increases in the chaotic regime. Standard deviations in the background and were obtained by sampling over  $N_{\text{step}} = 5 \times 10^4$  iterative steps. The inset in (c) magnifies the drop of the order parameter  $P_{\text{step}}$  with increasing low magnitude of  $K$  at constant density but varying total number of objects  $N$ .

see Eq. (6), as a function of the stochastic strength  $K$  are depicted in Fig. 7 for one stochastic realization for each value of  $K$ , yet after averaging over at least the last  $N_{\text{step}} = 5 \times 10^4$  time steps of each simulated realization.

For vanishing and low tendency of alignment  $A$ , see Fig. 7(a), we observe what might be expected from the Vicsek model. The whole crowd synchronizes for smaller stochastic strengths  $K$ . With growing values of  $K$ , this ordering breaks down.

Raising the tendency of alignment  $A$  into the regime of the first bifurcations in Fig. 3(a), see Fig. 7(b), the sensitivity with respect to the stochastic contributions increases when we increase  $A$  from 1.5 to 2.945. In principle, the stochastic influence on an object can push its angular orientation to another bifurcated branch. Overall, ordering is then affected. For the depicted values of  $K$ , the order parameter  $P_{\text{step}}$  remains at finite, nonvanishing magnitude, because in our consideration the stochastic contributions  $\Gamma_{i,n}$  are predominantly considered to arise from the mutual Vicsek-type alignment interactions between the objects. The stochastic terms are thus included before evaluating Eq. (1), as mentioned above. Therefore, the actual individual tendency of alignment due to

$A \neq 0$  in Eq. (1) remains and tends to drive all objects individually towards the preferred direction. As a result, nonvanishing overall orientational order  $P_{\text{step}}$  arises, despite the stochastic fluctuations in mutual alignment between the objects. Switching this order and adding the stochastic contributions only after evaluating Eq. (1), the curves, for instance, in Fig. 7(b) drop further towards zero with increasing  $K$ .

The trend of decaying order parameter  $P_{\text{step}}$  naturally becomes still more pronounced for tendencies of alignment  $A$  in the chaotic regime, see Figs. 7(c) and (d). Even if only weak deviations in the angular orientation of an individual object are caused by the stochastic contributions, they here according to Eq. (1) can result in significant angular deviations during subsequent time steps. A bias of this type strongly counteracts overall synchronization. Consequently, very weak stochastic influences can already induce a breakdown in overall alignment. The inset in Fig. 7(c) demonstrates that the drop in the order parameter  $P_{\text{step}}$  is still continuous at the considered system sizes at small magnitudes of the strength of stochastic contributions  $K$ . Yet, with increasing system size, that is, for increasing total number of objects  $N$  at identical overall density, the drop becomes steeper. At this point, we cannot exclude that an actual transition occurs from  $K = 0$  to  $K > 0$  for infinitely extended systems.

Interestingly, we observe a nonmonotonic curve in Fig. 7(d). After a steep decrease of the order parameter at very small amplitudes of fluctuations, it slightly recovers when we continue to increase the magnitude of fluctuations. Accordingly, in this chaotic example with significant overreaction, the presence of weak fluctuations can actually support ordering. Afterwards, with further increasing magnitude of fluctuations, the order parameter continues to decrease. Our analysis revealed that this nonmonotonic behavior is stable against moderate variations in the number of objects  $N$  and in the angular frequency  $\omega$ , see Figs. 8(a) and (b), respectively. However, the effect is significantly more sensitive with respect to changes in the strength of alignment tendency  $A$ , see Fig. 8(c). In Fig. 8(d), we confirm that the phenomenon is not associated with an insufficient amount of steps of iteration before evaluating the order parameter.

Briefly, we address the consequences of stochastic fluctuations during mutual alignment on the spatial concentration process indicated in Fig. 6(b). In that case, we observe a reduced trend of spatial concentration into one spot and of its correlated motion, as illustrated in the videos in the Supplemental Material [77]. Quantitatively, we have measured these trends using the order parameter  $P_{\text{loc}}$  as defined in Eq. (9). The results are illustrated in Fig. 9 in the chaotic regime for  $A = 5$  and  $A = 9.940441$ . Here, the increase (decrease) in  $P_{\text{loc}}$  is approximately correlated with the decrease (increase) in  $P_{\text{step}}$ . At  $K = 0$ , the low magnitude of  $P_{\text{loc}}$  indicates significant spatial concentration, which we have not observed for the other values of  $A$  studied in Fig. 7. At elevated values of  $K$ , the order parameter  $P_{\text{loc}}$  approaches the magnitude expected

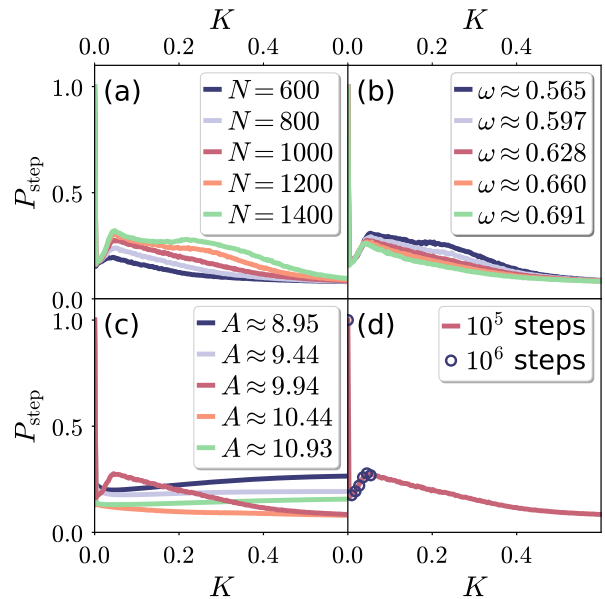


FIG. 8. Stability of the results in Fig. 7(d) against variations (a) in the number of objects  $N$ , (b) in the angular frequency  $\omega$ , (c) in the strength of alignment tendency  $A$ , and (d) in the number of steps of iteration before the order parameter  $P_{\text{step}}$  was recorded. Here, we set  $N_{\text{step}} = 5 \times 10^4$ , and in (d) the legend displays the overall number of iterative steps in that panel. Standard deviations are omitted for better visibility.

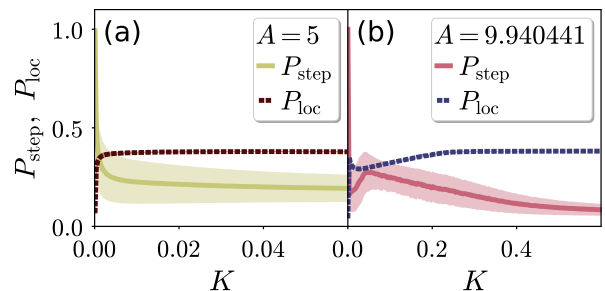


FIG. 9. Same as Figs. 7(c) and (d), but now amended by the magnitude of spatial concentration quantified by the order parameter  $P_{\text{loc}}$ , see Eq. (9). As in Figs. 7(c) and (d), the values of  $A$  are set to (a) 5 and (b) 9.940441, respectively. Standard deviations were obtained in the same way as indicated in the caption of Fig. 7 and here for  $P_{\text{loc}}$  at maximum are of the order of the line thickness.

for approximately equally spatially distributed objects in our system. An interesting question for future investigations concerns the relation between this spatial concentration and the propagating structures of high density emerging in regular Vicsek models [5, 78–80].

Finally, we consider the polydispersity of the actively driven objects as a source of disorder, instead of fluctuations in mutual alignment interactions. To this end, we concentrate on the tendency of alignment along  $-\hat{x}$ , parameterized by  $A$ . Specifically, before the angular and spatial initialization, we assign to each object a value  $A_i = A + \Gamma_{A,i}$  that is kept constant during the numerical

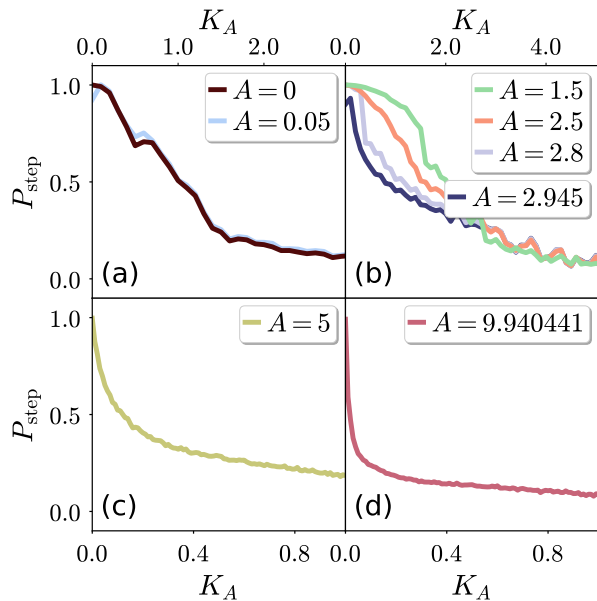


FIG. 10. Influence of the magnitude  $K_A$  of polydispersity in the tendency of alignment  $A$  on the resulting order parameter  $P_{\text{step}}$  in a crowd of  $N = 1000$  objects and  $\omega = \pi/5$ . One specific realization of polydispersity is addressed for each value of  $K_A$ . Again, for comparison, the values of  $A$  are set to (a) 0 and 0.05, (b) 1.5, 2.5, 2.8, and 2.945, (c) 5, and (d) 9.940441, as in Figs. 1(a), 2, 5, and 7–9. The sensitivity with respect to polydispersity apparently is more pronounced in the chaotic regime. Standard deviations obtained by averaging over five different realizations of the systems are mostly of the order of the line thickness or smaller.

iteration ( $i = 1, \dots, N$ ).  $\Gamma_{A,i}$  is drawn from a Gaussian distribution and uncorrelated between different objects, implying  $\langle \Gamma_{A,i} \rangle = 0$  and  $\langle \Gamma_{A,i} \Gamma_{A,j} \rangle = 2 K_A \delta_{ij}$ .

To evaluate the influence of polydispersity on our results, we increase  $K_A$  for the same values of  $A$  studied before in Figs. 1(a), 2, 5, and 7–9. Plotting the order parameter  $P_{\text{step}}$  as a function of increasing magnitude of polydispersity  $K_A$ , here for one different realization for each value of  $K_A$ , we infer from Fig. 10 similar qualitative trends as for increasing strengths of fluctuations in mutual angular alignment in Fig. 7, except for the nonmonotonic behavior in Fig. 7(d). However, quantitatively, the decrease in Fig. 10(b) is more substantially towards zero than in Fig. 7(b). Specifically when varying the tendency of alignment  $A$  for the individual objects in Fig. 10, different preferred individual angles of alignment result, see Fig. 3. In effect, this naturally reduces their overall orientational ordering as well, and  $P_{\text{step}}$  is reduced. Our example systems become particularly sensitive concerning polydispersity in the chaotic regime.

## VI. CONCLUSIONS

Summarizing, we have investigated the motion of self-propelled particles or actively driven objects that, when undisturbed, move in discrete steps along regular kinked trajectories. Rich nonlinear dynamics emerges when an additional tendency of alignment along a specified direction comes into play. We have observed discrete versions of cycloidal-like trajectories, straight motion under an oblique drift angle, various zigzag-like modes of migration, as well as chaotic motion in broad parameter intervals.

In fact, we found that this generic type of migration is associated with one of the most basic minimal models of nonlinear dynamics, namely, the Arnol'd circle map [66]. Through active transport, this nonlinear dynamics gets laid out into the two-dimensional plane in the form of the resulting trajectories. We always observe a net drift along a certain direction, even if comparatively weak and not necessarily along the requested orientation. Consequently, to reach a target at a certain remote location in combination with a set tendency towards circular trajectories, it generally becomes reasonable to work with an angular offset. Besides, the tendency of alignment must be tuned carefully.

This simple example demonstrates the richness that nonequilibrium and actively driven systems feature already in a very basic context. To observe the described effects in reality, nonsymmetric chiral hoppers driven through vibrating substrates can be biased towards one direction by gravity when inclining the vibrating plate [81, 82].

As a final remark, we mention that the picture of a drunk person trying to get home or to the next pub is frequently used to motivate the concept of a random walk. One may argue about whether this comparison is generally reasonable. After all, the person has a remote target and tries to reach it. Therefore, in view of our results, it may be more appropriate to reinterpret this type of motion of a person having the spins, performing discrete steps, and trying to reach a target as chaotic rather than random.

## ACKNOWLEDGMENTS

The author thanks the Deutsche Forschungsgemeinschaft (German Research Foundation, DFG) for support through the Heisenberg Grant No. ME 3571/4-1.

[1] T. Vicsek, A. Czirók, E. Ben-Jacob, I. Cohen, and O. Shochet, Novel type of phase transition in a system of

self-driven particles, Phys. Rev. Lett. **75**, 1226 (1995).  
[2] J. R. Howse, R. A. L. Jones, A. J. Ryan, T. Gough,



- R. Vafabakhsh, and R. Golestanian, Self-motile colloidal particles: from directed propulsion to random walk, *Phys. Rev. Lett.* **99**, 048102 (2007).
- [3] B. ten Hagen, S. van Teeffelen, and H. Löwen, Brownian motion of a self-propelled particle, *J. Phys.: Condens. Matter* **23**, 194119 (2011).
- [4] S. Henkes, Y. Fily, and M. C. Marchetti, Active jamming: self-propelled soft particles at high density, *Phys. Rev. E* **84**, 040301(R) (2011).
- [5] T. Ihle, Invasion-wave-induced first-order phase transition in systems of active particles, *Phys. Rev. E* **88**, 040303(R) (2013).
- [6] T. Speck, J. Bialké, A. M. Menzel, and H. Löwen, Effective Cahn-Hilliard equation for the phase separation of active Brownian particles, *Phys. Rev. Lett.* **112**, 218304 (2014).
- [7] J. Elgeti, R. G. Winkler, and G. Gompper, Physics of microswimmers—single particle motion and collective behavior: a review, *Rep. Prog. Phys.* **78**, 056601 (2015).
- [8] A. Zöttl and H. Stark, Emergent behavior in active colloids, *J. Phys.: Condens. Matter* **28**, 253001 (2016).
- [9] P. Romanczuk, H. Chaté, L. Chen, S. Ngo, and J. Toner, Emergent smectic order in simple active particle models, *New J. Phys.* **18**, 063015 (2016).
- [10] C. Jin, Y. Chen, C. C. Maass, and A. J. T. M. Mathijssen, Collective entrainment and confinement amplify transport by schooling microswimmers, *Phys. Rev. Lett.* **127**, 088006 (2021).
- [11] F. Kümmel, B. ten Hagen, R. Wittkowski, I. Buttinoni, R. Eichhorn, G. Volpe, H. Löwen, and C. Bechinger, Circular motion of asymmetric self-propelling particles, *Phys. Rev. Lett.* **110**, 198302 (2013).
- [12] B. ten Hagen, F. Kümmel, R. Wittkowski, D. Takagi, H. Löwen, and C. Bechinger, Gravitaxis of asymmetric self-propelled colloidal particles, *Nature Commun.* **5**, 1 (2014).
- [13] C. Bechinger, R. Di Leonardo, H. Löwen, C. Reichhardt, G. Volpe, and G. Volpe, Active particles in complex and crowded environments, *Rev. Mod. Phys.* **88**, 045006 (2016).
- [14] Y. Kubo, S. Inagaki, M. Ichikawa, and K. Yoshikawa, Mode bifurcation of a bouncing dumbbell with chirality, *Phys. Rev. E* **91**, 052905 (2015).
- [15] A. Deblais, T. Barois, T. Guerin, P.-H. Delville, R. Vaudaine, J. S. Lintuvuori, J.-F. Boudet, J.-C. Baret, and H. Kellay, Boundaries control collective dynamics of inertial self-propelled robots, *Phys. Rev. Lett.* **120**, 188002 (2018).
- [16] C. J. Brokaw, D. J. Luck, and B. Huang, Analysis of the movement of *Chlamydomonas* flagella: the function of the radial-spoke system is revealed by comparison of wild-type and mutant flagella., *J. Cell Biol.* **92**, 722 (1982).
- [17] R. Kamiya and G. B. Witman, Submicromolar levels of calcium control the balance of beating between the two flagella in demembrated models of *Chlamydomonas*, *J. Cell Biol.* **98**, 97 (1984).
- [18] E. Lauga, W. R. DiLuzio, G. M. Whitesides, and H. A. Stone, Swimming in circles: motion of bacteria near solid boundaries, *Biophys. J.* **90**, 400 (2006).
- [19] L. Lemelle, J.-F. Paliarne, E. Chatre, and C. Place, Counterclockwise circular motion of bacteria swimming at the air-liquid interface, *J. Bacteriol.* **192**, 6307 (2010).
- [20] R. Di Leonardo, D. Dell’Arciprete, L. Angelani, and V. Iebba, Swimming with an image, *Phys. Rev. Lett.* **106**, 038101 (2011).
- [21] L. Lemelle, J.-F. Paliarne, E. Chatre, C. Vaillant, and C. Place, Curvature reversal of the circular motion of swimming bacteria probes for slip at solid/liquid interfaces, *Soft Matter* **9**, 9759 (2013).
- [22] J. Hu, A. Wysocki, R. G. Winkler, and G. Gompper, Physical sensing of surface properties by microswimmers – directing bacterial motion via wall slip, *Sci. Rep.* **5**, 1 (2015).
- [23] A. Daddi-Moussa-Ider, M. Lisicki, S. Gekele, A. M. Menzel, and H. Löwen, Hydrodynamic coupling and rotational mobilities near planar elastic membranes, *J. Chem. Phys.* **149**, 014901 (2018).
- [24] T. Ohta and T. Ohkuma, Deformable self-propelled particles, *Phys. Rev. Lett.* **102**, 154101 (2009).
- [25] C. Krüger, G. Klös, C. Bahr, and C. C. Maass, Curling liquid crystal microswimmers: a cascade of spontaneous symmetry breaking, *Phys. Rev. Lett.* **117**, 048003 (2016).
- [26] M. Casiulis and D. Levine, Emergent synchronization and flocking in purely repulsive self-navigating particles, *Phys. Rev. E* **106**, 044611 (2022).
- [27] S. van Teeffelen and H. Löwen, Dynamics of a Brownian circle swimmer, *Phys. Rev. E* **78**, 020101(R) (2008).
- [28] M. Tarama and T. Ohta, Spinning motion of a deformable self-propelled particle in two dimensions, *J. Phys.: Condens. Matter* **24**, 464129 (2012).
- [29] H. Löwen, Chirality in microswimmer motion: from circle swimmers to active turbulence, *Eur. Phys. J. Spec. Top.* **225**, 2319 (2016).
- [30] C. Hoell, H. Löwen, and A. M. Menzel, Dynamical density functional theory for circle swimmers, *New J. Phys.* **19**, 125004 (2017).
- [31] B. Liebchen and D. Levis, Collective behavior of chiral active matter: pattern formation and enhanced flocking, *Phys. Rev. Lett.* **119**, 058002 (2017).
- [32] C. Kurzthaler and T. Franosch, Intermediate scattering function of an anisotropic Brownian circle swimmer, *Soft Matter* **13**, 6396 (2017).
- [33] G.-J. Liao and S. H. L. Klapp, Clustering and phase separation of circle swimmers dispersed in a monolayer, *Soft Matter* **14**, 7873 (2018).
- [34] L. Caprini and U. M. B. Marconi, Active chiral particles under confinement: surface currents and bulk accumulation phenomena, *Soft Matter* **15**, 2627 (2019).
- [35] Z.-F. Huang, A. M. Menzel, and H. Löwen, Dynamical crystallites of active chiral particles, *Phys. Rev. Lett.* **125**, 218002 (2020).
- [36] H. Löwen, Inertial effects of self-propelled particles: from active Brownian to active Langevin motion, *J. Chem. Phys.* **152**, 040901 (2020).
- [37] G.-J. Liao and S. H. L. Klapp, Emergent vortices and phase separation in systems of chiral active particles with dipolar interactions, *Soft Matter* **17**, 6833 (2021).
- [38] I. D. Couzin, J. Krause, R. James, G. D. Ruxton, and N. R. Franks, Collective memory and spatial sorting in animal groups, *J. Theor. Biol.* **218**, 1 (2002).
- [39] J. Buhl, D. J. T. Sumpter, I. D. Couzin, J. J. Hale, E. Despland, E. R. Miller, and S. J. Simpson, From disorder to order in marching locusts, *Science* **312**, 1402 (2006).
- [40] M. Ballerini, N. Cabibbo, R. Candelier, A. Cavagna, E. Cisbani, I. Giardina, V. Lecomte, A. Orlandi, G. Parisi, A. Procaccini, M. Viale, and V. Zdravkovic, Interaction ruling animal collective behavior depends on

- topological rather than metric distance: evidence from a field study, *Proc. Natl. Acad. Sci. U.S.A.* **105**, 1232 (2008).
- [41] K. Tunström, Y. Katz, C. C. Ioannou, C. Huepe, M. J. Lutz, and I. D. Couzin, Collective states, multistability and transitional behavior in schooling fish, *PLoS Comput. Biol.* **9**, e1002915 (2013).
- [42] D. L. Blair, T. Neicu, and A. Kudrolli, Vortices in vibrated granular rods, *Phys. Rev. E* **67**, 031303 (2003).
- [43] J. Deseigne, O. Dauchot, and H. Chaté, Collective motion of vibrated polar disks, *Phys. Rev. Lett.* **105**, 098001 (2010).
- [44] C. Scholz, A. Ldov, T. Pöschel, M. Engel, and H. Löwen, Surfactants and rotelles in active chiral fluids, *Science Adv.* **7**, eabf8998 (2021).
- [45] H. C. Berg and D. A. Brown, Chemotaxis in *Escherichia coli* analysed by three-dimensional tracking, *Nature* **239**, 500 (1972).
- [46] K. Y. Wan and R. E. Goldstein, Time irreversibility and criticality in the motility of a flagellate microorganism, *Phys. Rev. Lett.* **121**, 058103 (2018).
- [47] G. Grégoire and H. Chaté, Onset of collective and cohesive motion, *Phys. Rev. Lett.* **92**, 025702 (2004).
- [48] R. Kürsten and T. Ihle, Dry active matter exhibits a self-organized cross sea phase, *Phys. Rev. Lett.* **125**, 188003 (2020).
- [49] J. Codina, B. Mahault, H. Chaté, J. Dobnikar, I. Pagonabarraga, and X.-q. Shi, Small obstacle in a large polar flock, *Phys. Rev. Lett.* **128**, 218001 (2022).
- [50] A. M. Menzel, Unidirectional laning and migrating cluster crystals in confined self-propelled particle systems, *J. Phys.: Condens. Matter* **25**, 505103 (2013).
- [51] K. Schaller, R. David, and R. Uhl, How *Chlamydomonas* keeps track of the light once it has reached the right phototactic orientation, *Biophys. J.* **73**, 1562 (1997).
- [52] D. Helbing, I. Farkas, and T. Vicsek, Simulating dynamical features of escape panic, *Nature* **407**, 487 (2000).
- [53] A. C. H. Tsang, A. T. Lam, and I. H. Riedel-Kruse, Polygonal motion and adaptable phototaxis via flagellar beat switching in the microswimmer *Euglena gracilis*, *Nature Phys.* **14**, 1216 (2018).
- [54] L. Baraban, D. Makarov, O. G. Schmidt, G. Cuniberti, P. Leiderer, and A. Erbe, Control over Janus micromotors by the strength of a magnetic field, *Nanoscale* **5**, 1332 (2013).
- [55] L. Baraban, R. Streubel, D. Makarov, L. Han, D. Karnausenko, O. G. Schmidt, and G. Cuniberti, Fuel-free locomotion of Janus motors: magnetically induced thermophoresis, *ACS Nano* **7**, 1360 (2013).
- [56] A. F. Demirörs, M. T. Akan, E. Poloni, and A. R. Studart, Active cargo transport with Janus colloidal shuttles using electric and magnetic fields, *Soft Matter* **14**, 4741 (2018).
- [57] R. Blakemore, Magnetotactic bacteria, *Science* **190**, 377 (1975).
- [58] R. P. Blakemore, Magnetotactic bacteria, *Ann. Rev. Microbiol.* **36**, 217 (1982).
- [59] S. Klumpp and D. Faivre, Magnetotactic bacteria, *Eur. Phys. J. Spec. Top.* **225**, 2173 (2016).
- [60] R. E. Goldstein, M. Polin, and I. Tuval, Noise and synchronization in pairs of beating eukaryotic flagella, *Phys. Rev. Lett.* **103**, 168103 (2009).
- [61] C.-k. Tung, F. Ardon, A. Roy, D. L. Koch, S. S. Suarez, and M. Wu, Emergence of upstream swimming via a hydrodynamic transition, *Phys. Rev. Lett.* **114**, 108102 (2015).
- [62] A. J. T. M. Mathijssen, N. Figueroa-Morales, G. Junot, É. Clément, A. Lindner, and A. Zöttl, Oscillatory surface rheotaxis of swimming *E. coli* bacteria, *Nature Commun.* **10**, 1 (2019).
- [63] A. Attanasi, A. Cavagna, L. Del Castello, I. Giardina, T. S. Grigera, A. Jelić, S. Melillo, L. Parisi, O. Pohl, E. Shen, and M. Viale, Information transfer and behavioural inertia in starling flocks, *Nature Phys.* **10**, 691 (2014).
- [64] A. Cavagna, L. Del Castello, I. Giardina, T. Grigera, A. Jelic, S. Melillo, T. Mora, L. Parisi, E. Silvestri, M. Viale, and A. M. Walczak, Flocking and turning: a new model for self-organized collective motion, *J. Stat. Phys.* **158**, 601 (2015).
- [65] A. M. Menzel, Statistics for an object actively driven by spontaneous symmetry breaking into reversible directions, *J. Chem. Phys.* **157**, 011102 (2022).
- [66] V. I. Arnol'd, On analytic maps of the circle onto itself, in *Collected Works. Volume I. Representations of Functions, Celestial Mechanics, and KAM Theory 1957–1965*, edited by A. B. Givental, B. A. Khesin, J. E. Marsden, A. N. Varchenko, V. A. Vassilev, O. Y. Viro, and V. M. Zakalyukin (Springer, Berlin, Heidelberg, 2009) p. 212.
- [67] L. Glass and R. Perez, Fine structure of phase locking, *Phys. Rev. Lett.* **48**, 1772 (1982).
- [68] L. Glass, M. R. Guevara, A. Shrier, and R. Perez, Bifurcation and chaos in a periodically stimulated cardiac oscillator, *Physica D* **7**, 89 (1983).
- [69] S. Ostlund, D. Rand, J. Sethna, and E. Siggia, Universal properties of the transition from quasi-periodicity to chaos in dissipative systems, *Physica D* **8**, 303 (1983).
- [70] M. H. Jensen, P. Bak, and T. Bohr, Transition to chaos by interaction of resonances in dissipative systems. I. Circle maps, *Phys. Rev. A* **30**, 1960 (1984).
- [71] P. L. Boyland, Bifurcations of circle maps: Arnol'd tongues, bistability and rotation intervals, *Commun. Math. Phys.* **106**, 353 (1986).
- [72] T. Geisel and J. Nierwetberg, Onset of diffusion and universal scaling in chaotic systems, *Phys. Rev. Lett.* **48**, 7 (1982).
- [73] M. Schell, S. Fraser, and R. Kapral, Diffusive dynamics in systems with translational symmetry: a one-dimensional-map model, *Phys. Rev. A* **26**, 504 (1982).
- [74] G. Vásárhelyi, C. Virágh, G. Somorjai, T. Nepusz, A. E. Eiben, and T. Vicsek, Optimized flocking of autonomous drones in confined environments, *Science Robot.* **3**, eaat3536 (2018).
- [75] T. Bäuerle, A. Fischer, T. Speck, and C. Bechinger, Self-organization of active particles by quorum sensing rules, *Nature Commun.* **9**, 1 (2018).
- [76] F. A. Lavergne, H. Wendehenne, T. Bäuerle, and C. Bechinger, Group formation and cohesion of active particles with visual perception-dependent motility, *Science* **364**, 70 (2019).
- [77] See Supplemental Material at [URL will be inserted by publisher] for a video illustration of the dynamics indicated in Fig. 6(b) and for two additional videos for the same set-up, but for nonvanishing strengths of stochastic contributions  $K$ .
- [78] H. Chaté, F. Ginelli, G. Grégoire, and F. Raynaud, Collective motion of self-propelled particles interacting with a

- out cohesion, *Phys. Rev. E* **77**, 046113 (2008).
- [79] H. Chaté, F. Ginelli, G. Grégoire, F. Peruani, and F. Raynaud, Modeling collective motion: variations on the Vicsek model, *Eur. Phys. J. B* **64**, 451 (2008).
- [80] A. M. Menzel, Collective motion of binary self-propelled particle mixtures, *Phys. Rev. E* **85**, 021912 (2012).
- [81] P. S. Goohpattader and M. K. Chaudhury, Diffusive motion with nonlinear friction: apparently Brownian, *J. Chem. Phys.* **133**, 024702 (2010).
- [82] M. Mohammadi, K. Harth, D. Puzyrev, T. Hanselka, T. Trittel, and R. Stannarius, Dynamics of self-propelled particles passing a bottleneck, *New J. Phys.* **22**, 123025 (2020).